Journal of Digital Imaging (2023) 36:1633–1642
https://doi.org/10.1007/s10278-022-00764-y

Glomerulus Detection Using Segmentation Neural Networks

Surender Singh Samant[1] · **Arun Chauhan**[1] · **Jagadish DN**[2] · **Vijay Singh**[1]

Received: 7 April 2022 / Revised: 29 August 2022 / Accepted: 15 December 2022 / Published online: 5 April 2023

Abstract
Digital pathology is vital for the correct diagnosis of kidney before transplantation or kidney disease identification. One of the key challenges in kidney diagnosis is glomerulus detection in kidney tissue segments. In this study, we propose a deep learning–based method for glomerulus detection from digitized kidney slide segments. The proposed method applies models based on convolutional neural networks to detect image segments containing the glomerulus region. We employ various networks such as ResNets, UNet, LinkNet, and EfficientNet to train the models. In our experiments on a network trained on the NIH HuBMAP kidney whole slide image dataset, the proposed method achieves the highest scores with Dice coefficient of 0.942.

Keywords Glomerulus detection · Semantic segmentation · Convolutional neural networks · Kidney biopsy · Kidney transplantation

Introduction

Recently, the advances in deep learning (DL) techniques have impacted the field of medical imaging in a very significant manner. These advances have automated numerous medical procedures and have helped build robust medical and diagnostic applications. One such application is in the area of kidney transplantation. Before it can be transplanted, the donor's kidney has to be assessed for its fitness. Traditionally, trained pathologists analyze the donor's kidney visually during its biopsy examination. This process is not only time consuming but the high variability of observations among pathologists is also a major concern as it may result in quality organs discard.

✉ Surender Singh Samant
surender.samant@gmail.com

Arun Chauhan
aruntakhur@gmail.com

Jagadish DN
jagadishdn@gmail.com

Vijay Singh
vijaysingh.cse@geu.ac.in

[1] Department of Computer Science and Engineering, Graphic Era (Deemed to be University), Dehradun, 248002 Uttarkhand, India

[2] Department of Electronics and Communication Engineering, Indian Institute of Information Technology, Dharwad, Karnataka 580009, India

To mitigate this issue, whole slide scanners are used to facilitate the digitization of histopathological tissue and the recordings available as whole slide images (WSI). These images have a high resolution and are created from tissue slides. This enables the application of DL techniques in the virtual slides leading to the automation of pathology operations [1]. Therefore, it is desirable to to have artificial intelligence (AI)–based computer-aided diagnosis tools taking advantage of digital pathology to assist the decision-making process of pathologists.

Application of DL methods in the field of digital pathology is an active area of research. Specifically, convolutional neural networks (CNNs) are becoming increasingly important in WSI analysis as they have shown promising results in tasks such as pattern recognition and classification [2]. There is a great opportunity for CNNs in the area of digital pathology because of their ability to create features in an unsupervised manner. Furthermore, the availability of bigger datasets and many pre-trained deep learning models has also contributed to a significant increase in the popularity of DL techniques in digital pathology.

Glomerulus detection is critical in the field of nephropathology for accurate medical diagnosis. Glomeruli are capillary networks that take part in the first stage in the blood filtering process, retaining larger molecular weight proteins in blood circulation and resulting in urine production (see Fig. 1 for an illustration of a glomerulus). Any pathological alteration linked with glomeruli inside a tissue slice, such as the number or size of glomeruli, is a critical signal

for detecting illnesses in donors. Glomerulus formations exhibit a remarkable degree of diversity in size, shape, and color. Glomeruli in a healthy kidney, before sectioning, have a spherical shape, whose diameter ranges between 100 and 350μm, but their appearance might alter owing to the presence of medical disorders. Glomerulus, for example, might have a swollen appearance under hypertension [3] or diabetic condition [4]. Furthermore, the diameters of the visible glomerulus may vary depending on where the cross-section was taken in relation to each glomerulus sphere. Periodic acid-Schiff (PAS) stain in tissue slices gives the slides a purple-magenta color. The amount of stain in each slide determines the color intensity of the segments under examination. Because this technique is not flawless, different slides may have varying intensities. Furthermore, the existence of medical illnesses might affect the quantity of stain present in the glomeruli under investigation.

Researchers have used DL techniques to many similar medical classification tasks with interesting results. The research in [5] proposed a CNN model with handcrafted features for mitosis detection in breast cancer. The study in [6] deals with mitotic figure classification by combining manually designed nuclear features with learned features extracted by a CNN. The work in [7] uses very deep CNNs to classify diabetic retinopathy by configuring an 18-layered network. The authors in [8] use CNNs to exploit both local and global contextual features for brain tumor segmentation in MRI images. Many of the techniques proposed in the previous research have been used in glomurelus detection, but they suffer from limited accuracy [9]. The use of transfer learning has been found to have limited gain in the existing literature for glomerulus detection.

In this study, we concentrate on glomerulus detection using deep learning networks. We propose models that perform semantic segmentation on the WSIs. We evaluate the proposed models' ability to detect glomeruli using a metric called Dice coefficient. The main contributions of our work are:

- We propose segmentation using models such as UNet and LinkNet and pre-trained models such as EfficientNet and ResNet.
- We study various combinations of deep learning networks for glomerulus detection.
- Using the best combination in the proposed approach, we outperform the current state of the art and achieve the highest score in glomerulus detection.

The remainder of the paper is organized as follows. We discuss the related work in the "Related Work" section. In the "Methodology and Dataset" section, we explain the glomerulus detection method and various networks used for the detection. We present the experimental results for glomerulus detection in the "Experimental Results and Discussion" section. Finally, the "Conclusion and Future Work" section concludes the work and gives future direction.

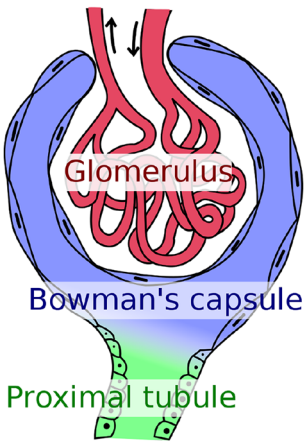

Fig. 1 Illustration of a glomerulus. By Mikael Häggström, used with permission

Related Work

Researchers have witnessed significant outcomes using DL techniques in tissue diagnosis. Methods for classifying and detecting glomeruli in the field of nephropathology have become critical in the area of disease diagnosis and research. Several recent studies have proposed computer-aided diagnostics systems for glomerulus detection and classification in renal biopsies [10–15]. The process of transplantation of a kidney retrieved from expanded criteria donors simply relies on a rushed histological examination of the organ to evaluate suitability for transplant [16]. Gallego et al. [10] proposed a glomerulus detection method based on the pre-trained AlexNet model [17]. Ledbetter et al. [11] proposed a CNN to infer the quantity of primary filtrate that passes from the blood through the glomerulus per minute by looking at the patients' WSI of their kidney biopsies. The authors in [18] focused on the segmentation of the glomeruli. They proposed two different CNN cascades for segmentation applications with sparse objects for glomerulus segmentation task and compared them with conventional fully convolutional network (FCN). Ma et al. [19] proposed employing a genetic algorithm for edge patching by using a Canny edge detector to get discontinuous edges of glomerulus and its final detection. The primary issue with this approach is that the boundaries identified by the Canny edge detector are not robust and are prone to mistakes when the color intensity varies. The authors of [20, 21] categorized glomeruli using the rectangular-histogram of gradients (R-HOG) [22] as a feature vector.

The issue with these approaches is that R-HOG has strict block division which leads to a high number of false positives. The research in [23] proposed the segmental HOG (S-HOG) as a potential candidate descriptor for glomerulus detection where the block division is not rigid. It used nine discretized oriented gradients and support vector machine (SVM) [24] as a supervised learning classifier to improve the R-HOG framework. In [25], a boundary identification method enhanced with the convex hull algorithm is used to analyze renal microscopic images. This technique identifies and categorizes glomeruli for the purpose of measuring diameter and Bowman's space thickness. The research in [26] introduced a method for detecting glomeruli based on the elliptical form of glomeruli to produce candidate areas. In the last phase, these areas are classified using a trained SVM classifier. In [27], a sliding window approach and SVM classifier were used to exploit features from HOG for glomerulus detection in WSIs with multiple stains. However, the results showed that the CNN outperformed the HOG and SVM classifier. The work in [13] employed a DL technique by using a faster R-CNN for glomerulus detection in multi-stained kidney biopsy. The work by [15] implemented a DL model to classify sclerotic and non-sclerotic glomeruli, given a WSI of frozen donor kidney biopsies. The method has a FCN in the front, followed by a blob detection algorithm [28], based on Laplacian-of-Gaussian, to post-process the FCN probability maps into object detection predictions. The research in [14] proposed a classification method on renal biopsies of patients with diabetic nephropathy. In the research, a combination of classical image processing and novel machine learning techniques was used. The authors of [29] utilized CNNs and created a network from an ensemble of five UNets for segmentation of ten tissue classes from WSIs of periodic acid-Schiff (PAS)–stained kidney transplant biopsies. The research in [30] utilized 3D magnetic resonance imaging (MRI) data to propose glomerulus detection using Hessian-based difference of Gaussians (HDoG) detector.

Methodology and Dataset

Figure 2 illustrates the glomerulus detection framework. The WSIs are in Tagged Image File Format (TIFF). We store the image and mask image tiles in the tfrecords format. The format has an array of images in the form of binary records and can be read efficiently while training the model. These images are fed to a glomerulus segmentation and detection model to train the network to perform segmentation.

Dataset

In this work, we use dataset from the NIH Human Biomolecular Atlas Program (HuBMAP) [31]. The dataset is around 40 GB in size consisting of a set of images. Each image is around 35k × 26k pixels in size with RGB 8-bit gamma integer colors, stored in TIFF. Each image contains thousands of glomerulus tissues. These images are taken from 11 fresh and frozen, and 9 formalin-fixed paraffin-embedded (FFPE) PAS kidneys. Figure 3a displays an image sample from the dataset.

Preprocessing

As the image size is very large, about 5 GB each, they consume significant amounts of memory. It is also very hard to load and process such large images.

RLE Decoding

Mask images are available in run length encoding (RLE) format. RLE is effective in data compression. As an example, 100 3 200 1 300 2 means take three pixels starting from 100, one pixel starting from 200 and two pixels starting from 300. The resulting mask is 100 101 102 200 300 301. We

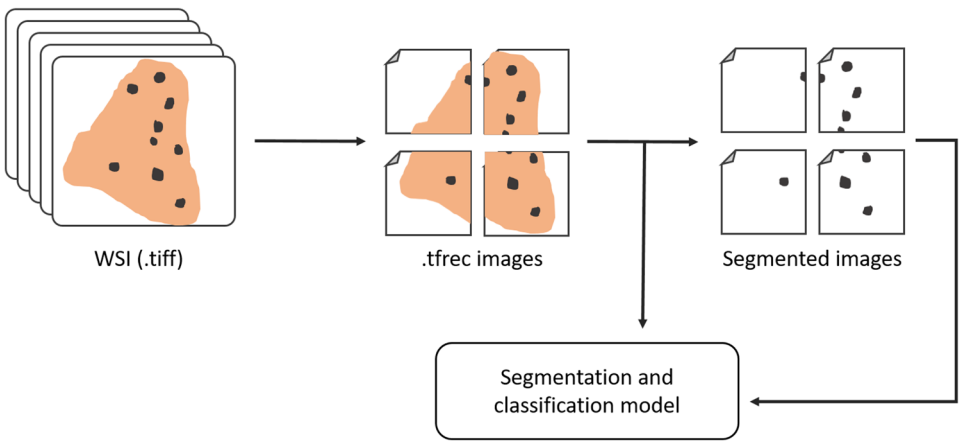

Fig. 2 Illustration of glomerulus segmentation and detection framework

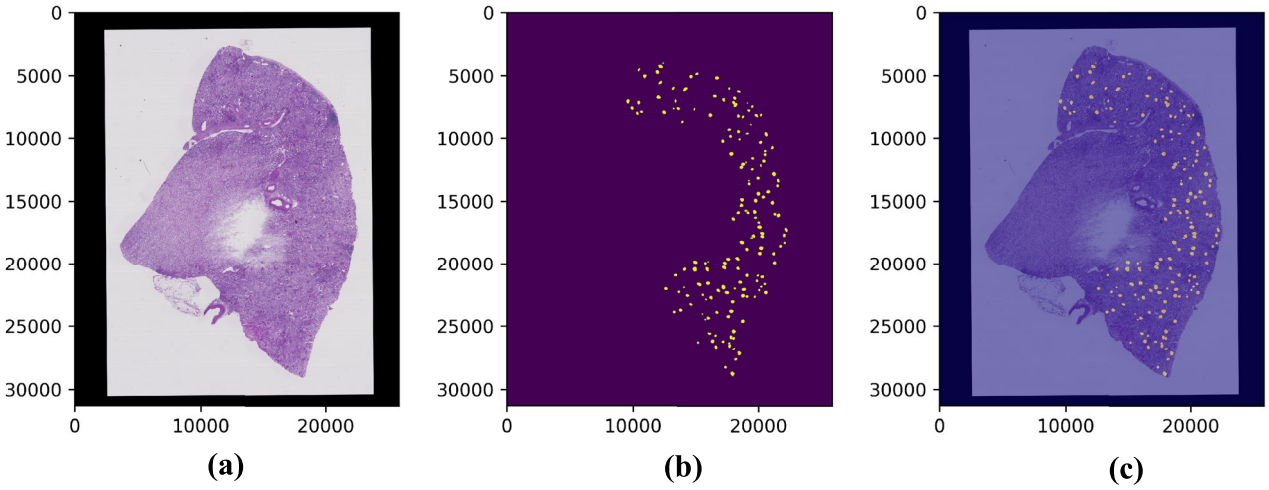

Fig. 3 Dataset sample: **a** kidney image, **b** RLE-decoded image mask, and **c** masked kidney image

convert RLE into images, and divide the large images into an array of smaller size images. Figure 3b shows an RLE-transformed mask image.

Masking

Image masking is the process of editing an image to highlight a few portions of the image, or to hide a few portions of the images. We use image masking to highlight the portions of the image where glomerulus is present. Figure 3c shows a mask applied on the kidney image.

Padding and Splitting

We add padding to all images and their corresponding mask images to be able to divide an image into small and equal sizes. The padding to an image and its corresponding mask image is the same because the mask image size is the same as the TIFF image. We divide the padded images and their corresponding mask images into smaller images like 1024×512 or 512×256 of equal size. We divide the image and mask from the same coordinate pixels. The split images are put into a format that machine learning models can process and analyze.

Figure 4 shows a sample split image having a glomerulus, the corresponding RLE-transformed mask, and the glomerulus-highlighted image.

Cleaning

Data cleaning is the process of preparing data for analysis by removing or modifying data that is incorrect, incomplete, irrelevant, duplicated, or improperly formatted. In this step, we check if the images are empty, and discard empty images.

Models

We conducted experiments with different types of neural networks to achieve the highest accuracy on the test data. For training, we used transfer learning techniques in which a previously trained model that has shown great results is applied on our dataset and the model's weights are modified accordingly. We used VGG19, InceptionV3, ResNet18, ResNet50, and a few versions of EfficientNet [32] as the pre-trained models. As segmentation networks, we used UNet [33], LinkNet [34], and FPN. The networks with the best results are described below.

UNet

Figure 5 shows the UNet architecture and operation descriptions. A specific encoder-decoder technique is used in this U-shaped architecture. In UNet, the encoder decreases the spatial dimensions in each layer while increasing the number of channels. The decoder, on the other hand, raises the spatial dimensions while decreasing the number of channels. The tensor that is sent into the decoder is a well-known bottleneck. Finally, the spatial dimensions are recovered in order to generate a forecast for each pixel in the input image. These kinds of models are often used in real-world applications.

LinkNet

The LinkNet structure, as depicted in Fig. 6, is based on the encoder-decoder architecture. It is a fully convolutional

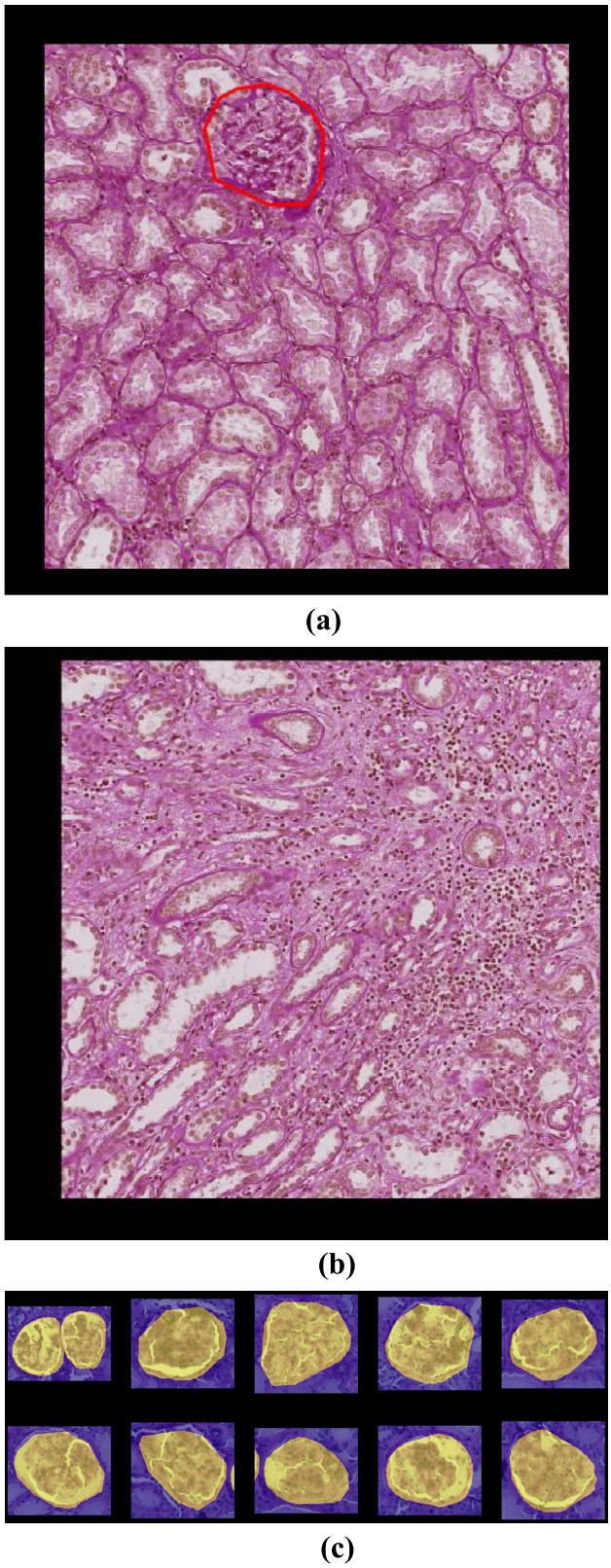

Fig. 4 Samples with **a** section of kidney image having a glomerulus, **b** section of kidney image having no glomeruli, and **c** masked glomerulus images

neural network for fast image semantic segmentation. It is a medium-sized, partially transfer-learned model as the encoder weights are pre-trained. LinkNet uses residuals in each of the encoder and decoder blocks. This makes it a fast and easy to train model. Here, both the encoder and decoder architectures are fully convolutional and they learn a pixel-to-pixel mapping for semantic segmentation. The ability to use pre-trained weights allows for greater flexibility and access to a richer set of image features for modeling the nonlinear segmentation function. The encoder architecture is the same as that of ResNet18 and it consists of four convolutional layers along with the residual networks. The first encoder block does not perform strided convolution and every convolution layer is followed by batch-normalization, and the rectified linear unit is used as non-linearity.

The initial block contains a convolution layer with a kernel size of 7×7 and a stride of 2. It is followed by a max-pooling layer with a window size of 2×2 and stride of 2. Similarly, the final block performs full convolution, taking feature maps from 64 to 32, followed by 2D-convolution. At the end, we use a full-convolution network as our classifier with a kernel size of 2×2.

EfficientNet

EfficientNet, shown in Fig. 7, is a convolutional neural network architecture developed by Google ([35]). This network proposed a novel approach to scale up convolutional neural networks. The conventional way of rescaling is to add layers. The EfficientNet model attempts systematic scaling of depth, width, and resolution of CNN. It uniformly scales all dimensions with a compound coefficient and balances dimensions of width/depth/resolution by scaling up with a constant ratio. For example, if we need 2^n more computational resources, then it may perform a^n depth increase, b^n height increase, and c^n image size increases where a, b, and c are constant coefficients that are determined by performing a small grid search on the original model. An important point to consider is that in convolution, due to the floating point operations (flops), doubling the width or resolution increases the flops 4 times. Scaling a convolution network with this equation will increase the flops by $a * b^2 * c^2$. The researchers constrained $a * b^2 * c^2 \approx 2$ such that for any new compound coefficient ϕ, there is approximately 2^ϕ increase in total flops. More layers are needed to increase the receptive field if the input image is bigger.

EfficientNetB0 was developed by the neural network itself. It optimizes both accuracy and floating-point operations. Taking the EfficientNetB0 as the baseline model, a full family of EfficientNetB1 to EfficientNetB7 were developed. EfficientNet gave greater accuracy of 84.4% on the ImageNet dataset. Its architecture uses mobile inverted

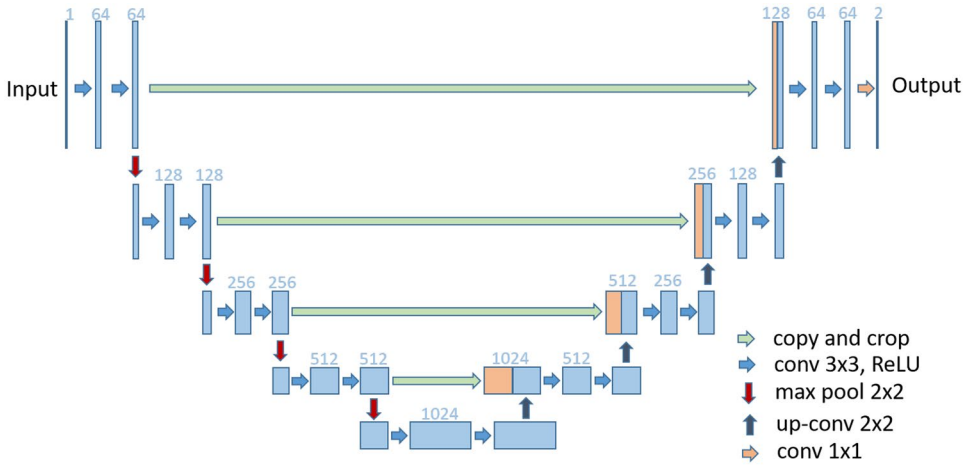

Fig. 5 UNet architecture

bottleneck convolution and it is slightly larger due to an increased FLOP budget.

EfficientNet's MB convolution block: It takes 2 inputs, one is data from the last layer and other is block arguments, a collection of attributes to be used inside an MB convolutional block like input filters, output filters, expansion ratio, and squeeze ratio. EfficientNet uses 7-MB convolution blocks where a block has kernel size for convolution, num_repeat that specifies how many times a particular block needs to be repeated and must be greater than zero, input_filters and output filters are numbers of specified filters, expand_ratio that is input filter expansion ratio, id_skip suggests whether to use skip connections or not, and se_ratio provides squeezing ratio for squeeze and excitation. It has an expansion phase, depthwise convolution phase, squeeze and excitation phase, and output phase.

Experimental Results and Discussion

As discussed in the "Methodology and Dataset" section, we conducted experiments with various kinds of neural networks to get the best possible results. We used a transfer learning technique so that the model's weights are fine-tuned during training. As pretrained models, we tried VGG19, InceptionV3, ResNet18, ResNet50, and a few versions of EfficientNet. For segmentation, we used UNet, LinkNet, and FPN. For details of the pretrained models and segmentation networks used, see the "Methodology and Dataset" section.

Metrics

Dice coefficient is a metric used to gauge the similarity of two samples [36]. Consider the square as a full image and A is the glomerulus cell to be detected. An illustration is shown in Fig. 8.

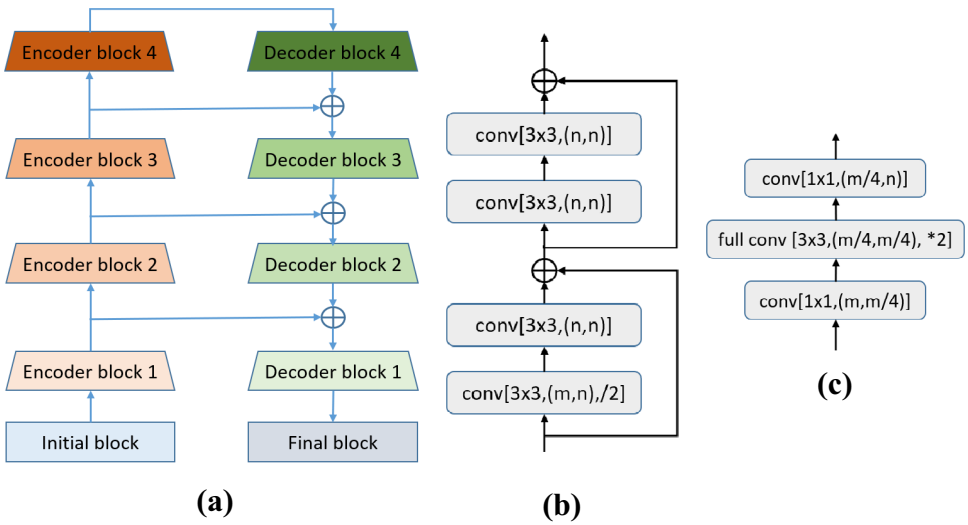

Fig. 6 LinkNet: **a** architecture, **b** encoder, **c** decoder

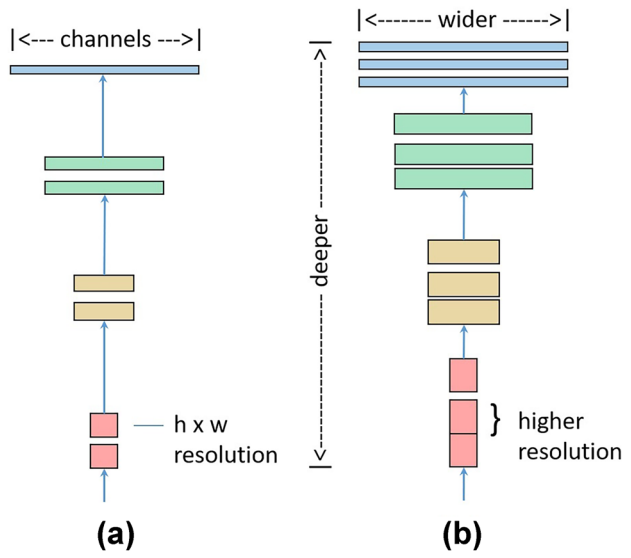

Fig. 7 EfficientNet architecture. **a** Baseline model. **b** Compound scaled model

In such a large image, the background occupies nearly 90% and foreground only 10%. In this type of biased dataset, normal accuracy metric does not represent the actual model capability. The Dice coefficient measures the match between the predicted segmentation of the model and the ground truth by comparing them in a pixel-wise manner.

Dice coefficient computes as two times the area of the intersection of images A and B, divided by the sum of the areas of A and B (1)

$$\text{Dice coefficient} = \frac{2 * |A \cap B|}{|A| + |B|} \quad (1)$$

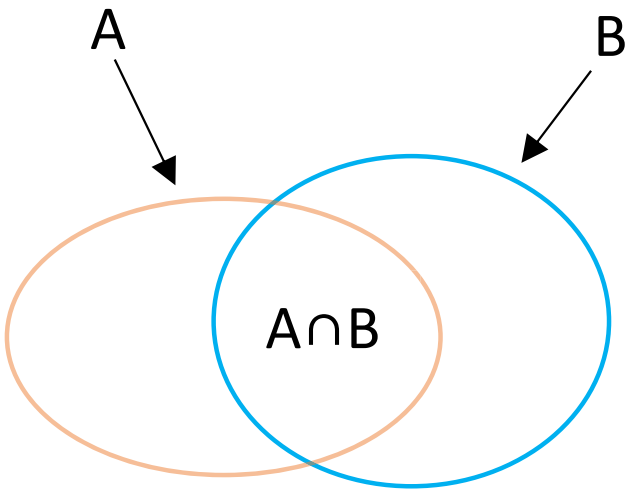

Fig. 8 Illustrative diagram to compute Dice coefficient

Test Results

We trained our model using many segmentation networks using various encoders with various types of parameters.We divided images into 1024×512 and 512×256 pixel sizes.

Network Trained on 1024×512 Size Images

We started with 1024×512 (performance of networks shown in Table 1) training on a UNet model with ResNet18 as a backbone network and then loaded weights of ImageNet; we could achieve Dice coefficient of 0.808. As can be seen in the results, the accuracy score is quite high but it does not reflect the true performance. We have shown accuracy scores for comparing it with the Dice coefficient metric. We later used ResNet50 instead of ResNet18 which has given 0.890. The ResNet backbone has not given greater results, so we used InceptionV3 as the backbone network and achieved the score of 0.901. We then trained UNet with EfficientNetB4 as the backbone network and achieved a score of 0.908. As we did not get better results with EfficientNet, we tried changing other parameters such as epochs and learning rate. Earlier we used 30 epochs, so we increased the number of epochs to 100. That improved the score to 0.913. We trained a few versions of EfficientNet using similar parameters and the UNet network, but the performance did not improve much with scores like 0.912, 0.913, and 0.914. We then started training on LinkNet for semantic segmentation. EfficientNetB4 achieved the score of 0.916; EfficientNetB6 scored 0.9417. We continued training all versions of EfficientNet with LinkNet as neural network. A LinkNet model with EfficientNetB3 as backbone network has given a Dice coefficient score of 0.942. Table 2 shows the confusion matrix

Table 1 Best performance of networks on 1024×512 size images

Network	Encoder	Accuracy	Dice coefficient
UNet	ResNet18 (30 epochs)	0.992	0.808
UNet	ResNet50 (30 epochs)	0.991	0.890
UNet	InceptionV3 (30 epochs)	0.992	0.901
UNet	EfficientNetB4 (30 epochs)	0.989	0.908
UNet	EfficientNetB3 (30 epochs)	0.994	0.892
UNet	VGG19 (100 epochs)	0.990	0.838
UNet	EfficientNetB4 (100 epochs)	0.996	0.916
UNet	EfficientNetB3 (100 epochs)	0.996	0.913
UNet	EfficientNetB2 (100 epochs)	0.996	0.912
UNet	EfficientNetB1 (100 epochs)	0.996	0.924
LinkNet	EfficientNetB4 (100 epochs)	0.996	0.916
LinkNet	EfficientNetB6 (100 epochs)	0.996	0.941
LinkNet	EfficientNetB3 (100 epochs)	**0.997**	**0.942**

Values in bold indicate the best scores

The scores we achieved used 30% of public dataset and 70% of private dataset

Table 2 Confusion matrix of the best performing proposed approach

	Foreground	Background
Foreground	.97	.03
Background	.02	.98

Table 3 Performance of networks on 512×256 size images

Network	Encoder	Accuracy	Dice coefficient
UNet	EfficientNetB1 (100 epochs)	0.995	0.902
UNet	EfficientNetB1 (1000 epochs)	0.995	0.903
LinkNet	EfficientNetB0 (1000 epochs)	0.996	0.938

The scores we achieved used 30% of public dataset and 70% of private dataset

of the results using our proposed approach. It can be seen that about 3% of the foreground pixels are classified as background, while 2% of background pixels are classified as foreground pixels.

Network Trained on 512 × 256 Size Images

With a 512 × 256 size image, the performance of networks is reported in Table 3. We trained the UNet model with EfficientNetB1 as the backbone network and scored a Dice coefficient of 0.903. The score is considerably low as the number of epochs was only 100, which is less for this case. After increasing the number of epochs to 1000 with EfficientNetB1, we could achieve 0.903. UNet could not give greater results. So we started training using the LinkNet model with EfficientNetB0 as the backbone network. This gave the score of 0.938. We have achieved the best score with 1024 × 512 image tiles using LinkNet as a model with EfficientNetB0 as the backbone network.

Comparison with State-of-the-Art

We now compare our approach with the current state of the art, namely *SegNet* and *Deeplab*. Table 4 depicts the results in the glomerulus detection task. SegNet is a segmentation architecture composed of an encoder network and a corresponding decoder network, followed by a final pixel-wise classification layer. SegNet does not learn the upsampling process as the indices used in the max-pooling step in the encoder are stored and applied back when upsampling in the corresponding layers of the decoder. Deeplab involves dilated convolution. The network consents to broaden the field of view of filters to incorporate a larger context. It can be seen that the proposed approach has the highest score.

Table 4 Comparison of the proposed methods with the current state-of-the-art

Work	Network	Dice coefficient
[15]	FCN + blob-detection	0.848
[37]	SegNet	0.859
[37]	Deeplab v3+	0.924
Our	Linknet + EfficientNetB3	0.942

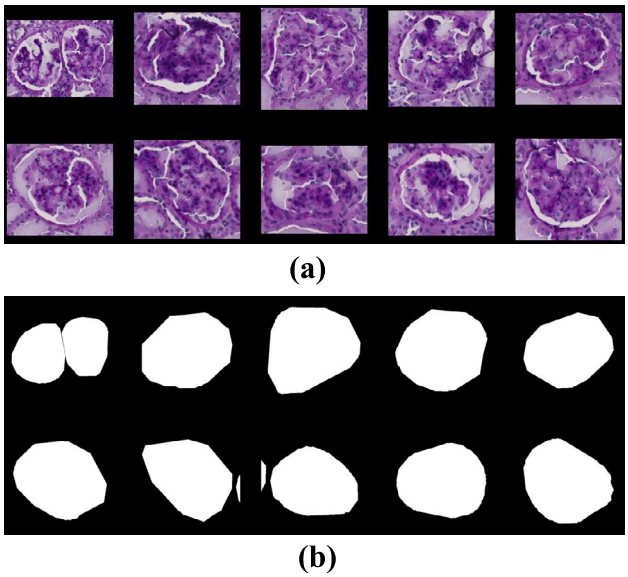

Fig. 9 Sample results of semantic segmentation. The zoomed glomureli are shown in **a**, while their semantic segmentation is shown in **b**

Figure 9 shows examples of glomureli and their semantic segmentation using the proposed approach.

Conclusion and Future Work

In this work, we proposed a method for glomerulus detection from the whole slide images of kidney tissue. The large-sized images undergo masking and slicing to yield smaller sized images, on which the deep learning networks are trained. Out of multiple segmentation networks that were trained, LinkNet with EfficientNet variants achieved promising results. LinkNet + EfficientNetB0 achieves the highest scores on 512 × 256 pixel size image tiles, while LinkNet + EfficientNetB3 scored the highest on 1024 × 512 pixel size image tiles. As future work, the proposed method will be validated on even more types of image datasets. Another future work is to experiment with more deep learning models to further improve glomerulus detection performance.

Author Contribution All the authors contributed equally to the study. All the authors read and approved the final manuscript.

Data Availability The results obtained in this paper are based upon data generated by the NIH Human BioMolecular Atlas Program (HuBMAP). The images used in the paper are available at https://portal.hubmapconsortium.org.

Declarations

Competing Interests The authors declare no competing interests.

References

1. Bueno, G., Fernandez-Carrobles, M.M., Deniz, O., Garca-Rojo, M.: New trends of emerging technologies in digital pathology. Pathobiology 83(2-3), 61–69 (2016)
2. Janowczyk, A., Madabhushi, A.: Deep learning for digital pathology image analysis: A comprehensive tutorial with selected use cases. Journal of pathology informatics 7 (2016)
3. Hughson, M.D., Puelles, V.G., Hoy, W.E., Douglas-Denton, R.N., Mott, S.A., Bertram, J.F.: Hypertension, glomerular hypertrophy and nephrosclerosis: the effect of race. Nephrology Dialysis Transplantation 29(7), 1399–1409 (2014)
4. Rasch, R., Lauszus, F., Thomsen, J.S., Flyvbjerg, A.: Glomerular structural changes in pregnant, diabetic, and pregnant-diabetic rats. Apmis 113(7-8), 465–472 (2005)
5. Wang, H., Roa, A.C., Basavanhally, A.N., Gilmore, H.L., Shih, N., Feldman, M., Tomaszewski, J., Gonzalez, F., Madabhushi, A.: Mitosis detection in breast cancer pathology images by combining handcrafted and convolutional neural network features. Journal of Medical Imaging 1(3), 034003 (2014)
6. Malon, C.D., Cosatto, E.: Classification of mitotic figures with convolutional neural networks and seeded blob features. Journal of pathology informatics 4 (2013)
7. Xu, K., Zhu, L., Wang, R., Liu, C., Zhao, Y.: Su-f-j-04: Automated detection of diabetic retinopathy using deep convolutional neural networks. Medical Physics 43(6Part8), 3406–3406 (2016)
8. Havaei, M., Davy, A., Warde-Farley, D., Biard, A., Courville, A., Bengio, Y., Pal, C., Jodoin, P.-M., Larochelle, H.: Brain tumor segmentation with deep neural networks. Medical image analysis 35, 18–31 (2017)
9. Lee, H.-C., Aqil, A.F.: Combination of transfer learning methods for kidney glomeruli image classification. Applied Sciences 12(3) (2022). https://doi.org/10.3390/app12031040
10. Gallego, J., Pedraza, A., Lopez, S., Steiner, G., Gonzalez, L., Laurinavicius, A., Bueno, G.: Glomerulus classification and detection based on convolutional neural networks. Journal of Imaging 4(1), 20 (2018)
11. Ledbetter, D., Ho, L., Lemley, K.V.: Prediction of kidney function from biopsy images using convolutional neural networks. arXiv preprint arXiv:1702.01816 (2017)
12. Cascarano, G.D., Debitonto, F.S., Lemma, R., Brunetti, A., Buongiorno, D., De Feudis, I., Guerriero, A., Rossini, M., Pesce, F., Gesualdo, L., : An innovative neural network framework for glomerulus classification based on morphological and texture features evaluated in histological images of kidney biopsy. In: International Conference on Intelligent Computing, pp. 727–738 (2019). Springer
13. Kawazoe, Y., Shimamoto, K., Yamaguchi, R., Shintani-Domoto, Y., Uozaki, H., Fukayama, M., Ohe, K.: Faster r-cnn-based glomerular detection in multistained human whole slide images. Journal of Imaging 4(7), 91 (2018)
14. Ginley, B., Lutnick, B., Jen, K.-Y., Fogo, A.B., Jain, S., Rosenberg, A., Walavalkar, V., Wilding, G., Tomaszewski, J.E., Yacoub, R., : Computational segmentation and classification of diabetic glomerulosclerosis. Journal of the American Society of Nephrology 30(10), 1953–1967 (2019)
15. Marsh, J.N., Matlock, M.K., Kudose, S., Liu, T.-C., Stappenbeck, T.S., Gaut, J.P., Swamidass, S.J.: Deep learning global glomerulosclerosis in transplant kidney frozen sections. IEEE transactions on medical imaging 37(12), 2718–2728 (2018)
16. Karpinski, J., Lajoie, G., Cattran, D., Fenton, S., Zaltzman, J., Cardella, C., Cole, E.: Outcome of kidney transplantation from high-risk donors is determined by both structure and function. Transplantation 67(8), 1162–1167 (1999)
17. Krizhevsky, A., Sutskever, I., Hinton, G.E.: Imagenet classification with deep convolutional neural networks. Advances in neural information processing systems 25, 1097–1105 (2012)
18. Gadermayr, M., Dombrowski, A.-K., Klinkhammer, B.M., Boor, P., Merhof, D.: CNN cascades for segmenting whole slide images of the kidney. CoRR (2017)
19. Ma, J., Zhang, J., Hu, J.: Glomerulus extraction by using genetic algorithm for edge patching. In: 2009 IEEE Congress on Evolutionary Computation, pp. 2474–2479 (2009). IEEE
20. Hirohashi, Y., Relator, R., Kakimoto, T., Saito, R., Horai, Y., Fukunari, A., Kato, T.: Automated quantitative image analysis of glomerular desmin immunostaining as a sensitive injury marker in spontaneously diabetic torii rats. J Biomed Image Process 1(1), 20–8 (2014)
21. Kakimoto, T., Okada, K., Fujitaka, K., Nishio, M., Kato, T., Fukunari, A., Utsumi, H.: Quantitative analysis of markers of podocyte injury in the rat puromycin aminonucleoside nephropathy model. Experimental and Toxicologic Pathology 67(2), 171–177 (2015)
22. Dalal, N., Triggs, B.: Histograms of oriented gradients for human detection. In: 2005 IEEE Computer Society Conference on Computer Vision and Pattern Recognition (CVPR'05), vol. 1, pp. 886–893 (2005). Ieee
23. Kato, T., Relator, R., Ngouv, H., Hirohashi, Y., Takaki, O., Kakimoto, T., Okada, K.: Segmental hog: new descriptor for glomerulus detection in kidney microscopy image. Bmc Bioinformatics 16(1), 1–16 (2015)
24. Boser, B.E., Guyon, I.M., Vapnik, V.N.: A training algorithm for optimal margin classifiers. In: Proceedings of the Fifth Annual Workshop on Computational Learning Theory, pp. 144–152 (1992)
25. Kotyk, T., Dey, N., Ashour, A.S., Balas-Timar, D., Chakraborty, S., Ashour, A.S., Tavares, J.M.R.: Measurement of glomerulus diameter and bowman's space width of renal albino rats. Computer methods and programs in biomedicine 126, 143–153 (2016)
26. Marée, R., Dallongeville, S., Olivo-Marin, J.-C., Meas-Yedid, V.: An approach for detection of glomeruli in multisite digital pathology. In: 2016 IEEE 13th International Symposium on Biomedical Imaging (ISBI), pp. 1033–1036 (2016). IEEE
27. Temerinac-Ott, M., Forestier, G., Schmitz, J., Hermsen, M., Bräsen, J., Feuerhake, F., Wemmert, C.: Detection of glomeruli in renal pathology by mutual comparison of multiple staining modalities. In: Proceedings of the 10th International Symposium on Image and Signal Processing and Analysis, pp. 19–24 (2017). IEEE
28. Lindeberg, T.: Detecting salient blob-like image structures and their scales with a scale-space primal sketch: A method for focus-of-attention. International Journal of Computer Vision 11(3), 283–318 (1993)
29. Hermsen, M., de Bel, T., Den Boer, M., Steenbergen, E.J., Kers, J., Florquin, S., Roelofs, J.J., Stegall, M.D., Alexander, M.P., Smith, B.H., : Deep learning–based histopathologic assessment of kidney tissue. Journal of the American Society of Nephrology 30(10), 1968–1979 (2019)
30. Zhang, M., Wu, T., Bennett, K.M.: A novel hessian based algorithm for rat kidney glomerulus detection in 3d mri. In: Medical

Imaging 2015: Image Processing, vol. 9413, p. 94132 (2015). International Society for Optics and Photonics
31. Consortium, H., : The human body at cellular resolution: the NIH human biomolecular atlas program. Nature 574(7777), 187 (2009)
32. Tan, M., Le, Q.: Efficientnet: Rethinking model scaling for convolutional neural networks. In: International Conference on Machine Learning, pp. 6105–6114 (2019). PMLR
33. Ronneberger, O., Fischer, P., Brox, T.: U-net: Convolutional networks for buomedical image segmentation. In: International Conference on Medical Image Computing and Computer-assisted Intervention, pp. 234–241 (2015). Springer
34. Chaurasia, A., Culurciello, E.: Linknet: Exploiting encoder representations for efficient semantic segmentation. In: 2017 IEEE Visual Communications and Image Processing (VCIP), pp. 234–241 (2017). IEEE
35. Tan, M., Le, Q.V.: Efficientnet: Rethinking model scaling for convolutional neural networks. In: Chaudhuri, K., Salakhutdinov, R. (eds.) Proceedings of the 36th International Conference on Machine Learning, ICML 2019, 9-15 June 2019, Long Beach, California, USA. Proceedings of Machine Learning Research, vol. 97, pp. 6105–6114. PMLR, ??? (2019). http://proceedings.mlr.press/v97/tan19a.html
36. Tustison, N., Gee, J.: Introducing dice, jaccard, and other label overlap measures to ITK. Insight J 2 (2009)
37. Altini, N., Cascarano, G.D., Brunetti, A., Marino, F., Rocchetti, M.T., Matino, S., Venere, U., Rossini, M., Pesce, F., Gesualdo, L., Bevilacqua, V.: Semantic segmentation framework for glomeruli detection and classification in kidney histological sections. Electronics 9(3), 503 (2020)